THE JOURNAL OF PHYSICAL CHEMISTRY C
Article
pubs.acs.org/JPCC

The Parameter Space of Graphene Chemical Vapor Deposition on Polycrystalline Cu

Piran R. Kidambi,[†] Caterina Ducati,[‡] Bruno Dlubak,[†] Damian Gardiner,[†] Robert S. Weatherup,[†] Marie-Blandine Martin,[§,∥] Pierre Seneor,[§,∥] Harry Coles,[†] and Stephan Hofmann*[,†]

[†]Department of Engineering, University of Cambridge, Cambridge CB3 0FA, United Kingdom

[‡]Department of Materials Science and Metallurgy, University of Cambridge, Cambridge CB2 3QZ, United Kingdom

[§]Unité Mixte de Physique CNRS/Thales, 91767 Palaiseau, France

[∥]Université de Paris-Sud 11, 91405 Orsay, France

Supporting Information

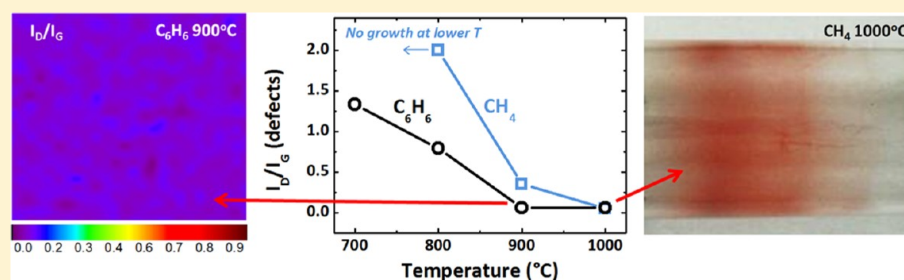

ABSTRACT: A systematic study of the parameter space of graphene chemical vapor deposition (CVD) on polycrystalline Cu foils is presented, aiming at a more fundamental process rationale in particular regarding the choice of carbon precursor and mitigation of Cu sublimation. CH_4 as precursor requires H_2 dilution and temperatures ≥1000 °C to keep the Cu surface reduced and yield a high-quality, complete monolayer graphene coverage. The H_2 atmosphere etches as-grown graphene; hence, maintaining a balanced CH_4/H_2 ratio is critical. Such balance is more easily achieved at low-pressure conditions, at which however Cu sublimation reaches deleterious levels. In contrast, C_6H_6 as precursor requires no reactive diluent and consistently gives similar graphene quality at 100−150 °C lower temperatures. The lower process temperature and more robust processing conditions allow the problem of Cu sublimation to be effectively addressed. Graphene formation is not inherently self-limited to a monolayer for any of the precursors. Rather, the higher the supplied carbon chemical potential, the higher the likelihood of film inhomogeneity and primary and secondary multilayer graphene nucleation. For the latter, domain boundaries of the inherently polycrystalline CVD graphene offer pathways for a continued carbon supply to the catalyst. Graphene formation is significantly affected by the Cu crystallography; i.e., the evolution of microstructure and texture of the catalyst template form an integral part of the CVD process.

■ INTRODUCTION

Economic, large-area growth combined with viable front and back-end integration strategies of monolayer and few-layer graphene (M/FLG) are key requirements for the commercial exploitation of graphene's unique properties. Chemical vapor deposition (CVD) is the most promising route toward M/FLG production and integration, based on its versatility and success with other nanomaterials.[1−3] While progress has been made in achieving MLG CVD over large areas,[4,5] the underlying growth mechanisms have yet to be fully understood[6−8] and the often narrow empirical process optimizations allow little generalization due to the vast CVD parameter space.[4,5,9−13] Most current literature focuses on exposing polycrystalline Cu[4,5,9−13] foils to methane (CH_4) at low pressures (LPs) and high temperatures (≥1000 °C). As-grown graphene can be fully continuous, but is inherently polycrystalline,[10] with MLG domain sizes typically ≤5 μm in dimension.[10−12] Recent efforts have focused on increasing the MLG domain size,[12,13] but in general the compromise made to achieve high-quality CVD graphene is to face undesirably high levels of Cu sublimation.[14]

Here, we focus on understanding graphene formation on polycrystalline Cu foils via a systematic exploration of the wider CVD parameter space, in particular regarding the choice of carbon precursor and mitigation of Cu sublimation, aiming at more rational process design. For CH_4 as precursor we find that, in agreement with previous literature,[4,5,9−12] uniform, high-quality MLG growth is restricted to a rather narrow CVD parameter set of LP conditions, H_2 dilution, and temperatures ≥1000 °C, at which Cu sublimation is at deleterious levels. The H_2 atmosphere is required to keep the Cu surface reduced, but

Received: April 14, 2012
Revised: September 24, 2012
Published: September 27, 2012

ACS Publications © 2012 American Chemical Society

dx.doi.org/10.1021/jp303597m | J. Phys. Chem. C 2012, 116, 22492−22501

at the same time can etch as-grown graphene. Hence, maintaining a balanced CH_4/H_2 ratio is critical, which makes the CH_4-based CVD process so delicate. In contrast, we find that benzene (C_6H_6) as precursor requires no reactive diluent, i.e., no delicate balance to be maintained, and consistently gives similar graphene quality at 100−150 °C lower temperatures compared to CH_4-based CVD. The lower process temperature and more robust processing conditions allow the problem of Cu sublimation to be effectively addressed. Our growth study shows that Cu-catalyzed CVD graphene formation is not inherently self-limited to a monolayer. Rather, we find the nucleation density, percentage of multilayer nuclei, and film uniformity/quality to critically depend on CVD conditions and growth kinetics. We suggest that the domain boundaries and other defects of the inherently polycrystalline CVD graphene offer pathways for the precursor to reach the catalyst even after complete MLG coverage. Our data further emphasize that the Cu catalyst template is not static and that the involved kinetics of grain growth are highly process dependent, making this an important process step for controlled graphene CVD.

EXPERIMENTAL METHODS

Graphene synthesis is carried out in a customized cold-wall, low-pressure CVD (LPCVD) reactor (a heavily modified Aixtron BM3, base pressure ∼5×10^{-6} mbar) and a hot-wall, atmospheric-pressure furnace (APCVD). For LPCVD the total pressure (0.001−100 mbar) was regulated by a pressure controller at the reactor outlet. Commercial, cold-rolled Cu foils of different thicknesses and purities (Alfa Aesar Puratronic, 99.999% purity, 25 and 100 μm thick; Advent Research Materials, 99.995% purity, 12 μm thick) are used as catalysts. A one-step CVD recipe is used as a benchmark process for all systems. For all CVD recipes, heating and preannealing is carried out in H_2 at 1000 °C (LPCVD, 4 mbar total pressure, heating rate ∼250 °C/min to 800 °C followed by 50 °C/min to 1000 °C; APCVD, heating rate ∼40 °C/min), after which the temperature is stabilized at the chosen growth temperature. In the case of CH_4 as the precursor, CH_4 is added to the annealing gas and cooling is performed in pure Ar (LPCVD cooling ramp ∼150 °C/min to 400 °C at 7 mbar, APCVD cooling rate ∼30 °C/min). For C_6H_6 LPCVD, the exposure is to C_6H_6 (>99.7% purity, Sigma-Aldrich) without H_2 and cooling is performed in a vacuum.

Samples were characterized by scanning electron microscopy (SEM; Philips XL30, 1−2 kV) and Raman spectroscopy (Renishaw InVia spectrometer, 532 nm excitation). For the latter the M/FLG was typically transferred to SiO_2 (300 nm)/Si substrates using a poly(methyl methacrylate) (PMMA) support layer and a 0.5 M aqueous solution of $FeCl_3$ to etch the Cu foil. Acetone was then used to dissolve the PMMA support. Hall-bar devices were fabricated via e-beam lithography. Graphene layers, transferred to SiO_2/Si wafer substrates, were etched by an O_2 plasma and Au/Ti contacts evaporated on top. All electrical measurements were performed at room temperature. Electron backscattered diffraction (EBSD) experiments were performed in an FEI Helios dual-beam microscope (5−15 kV, current ∼5.5 nA, working distance ∼5−6.5 mm, and sample tilt of ∼60° with respect to the electron beam) with an Oxford Instruments HKL EBSD Nordlys II detector in spot mode using Channel 5 software. Birefringence measurements followed the method outlined by Kim et al.[15] Liquid crystals of 4-pentyl-4′-cyanobiphenyl (5CB; Merck GmbH) were drop cast onto graphene transferred to a glass substrate. A thin coverslip was added on top, and measurements were carried out with the as-prepared sample placed between two crossed polarizers on a rotatable stage.

RESULTS

The process of graphene formation on metal surfaces in general comprises nucleation, a subsequent expansion of the nuclei into domains, followed by a merging of the domains into a continuous covalently bonded film.[16] Here we refer to domains as regions that grow from a single nucleation point. Figure 1 shows SEM images of the Cu surface after short CH_4/H_2 exposures (see process details in the caption), i.e., the early stages of CVD before the graphene coverage is continuous. Clear differences can already be seen for the different CVD

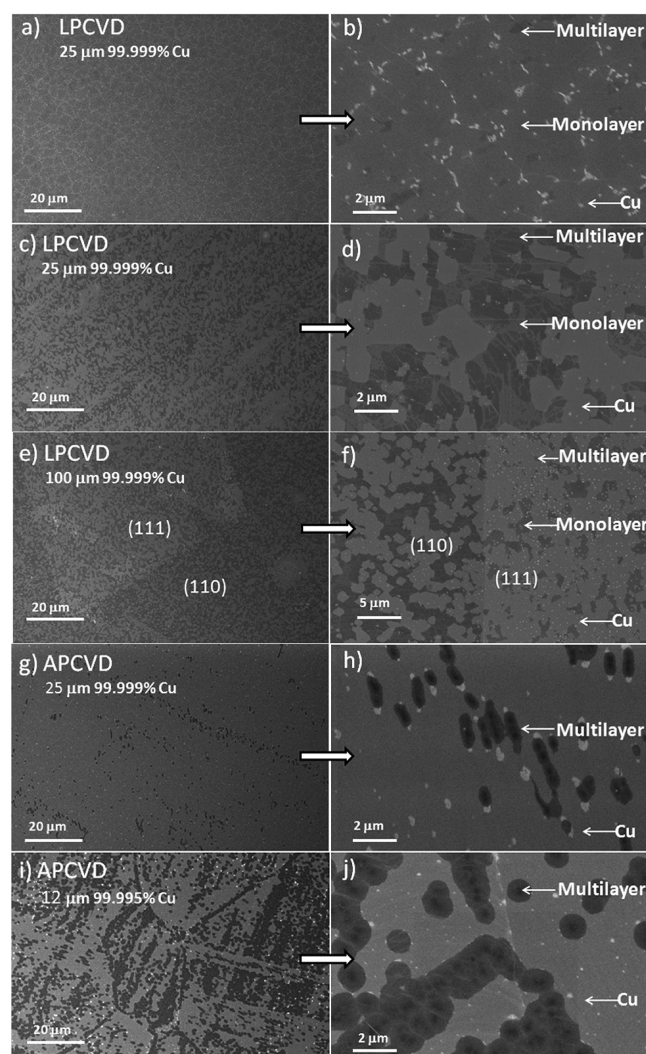

Figure 1. SEM images at different magnifications showing graphene nuclei on Cu before merging to form a continuous film: (a, b) monolayer nuclei, LPCVD, 4 mbar, 1000 °C, 1:10 CH_4/H_2 for 25 min, before merging to form a continuous film on 99.999% pure 25 μm foil, (c, d) multilayer nuclei, LPCVD, 4 mbar, 1000 °C, 1:1 CH_4/H_2 for 5 min, on 99.999% pure 25 μm foil, (e, f) multilayer nuclei, LPCVD, 4 mbar, 1000 °C, 1:1 CH_4/H_2 for 5 min, on 99.999% pure 100 μm foil with the underlying Cu grain orientation measured by EBSD, (g, h) multilayer nuclei, APCVD, 1000 °C, 1:25 CH_4/H_2 for 5 min, on 99.999% pure 25 μm foil, (i, j) multilayer nuclei, APCVD, 1000 °C, 1:25 CH_4/H_2 for 5 min, on 99.995% pure 12 μm Cu foil.

conditions. Parts a,b and parts c,d of Figure 1 compare low (1:10) and high (1:1) CH_4/H_2 ratios for LPCVD conditions. For the former we observe MLG domains ranging from typically ~30 to 40 μm^2 in size, with a few isolated areas (2−4 μm^2) of FLG (as seen by SEM contrast and confirmed by Raman spectroscopy; see below). This is largely consistent with recent literature on optimized CVD with CH_4 on Cu foils.[4,5,9−13] We note that, due to the pressure regulation and backfilling procedure, the CH_4/H_2 ratio for our process is initially lower at the point of CH_4 addition and thus partly resembles two-step exposures reported in the literature.[17] A higher CH_4 partial pressure (Figure 1c,d) leads to predominantly multilayer graphene nucleation and decreased sample homogeneity. This highlights that, at the initial stages of growth, which we refer to as the primary nucleation stage, Cu is not inherently limiting graphene formation to a monolayer.

Parts e−j of Figure 1 highlight that the nature of graphene nucleation and growth at the early stages is highly dependent on the catalyst surface orientation and impurity levels. Parts e,f of Figure 1 show that for the same CVD conditions the resultant graphene coverage is different on adjacent Cu facets, with the imaged Cu(111) surface showing less graphene coverage compared to the Cu(110) surface. APCVD conditions as in Figure 1g−j result in a predominantly multilayer nucleation pattern. The nucleation density is notably increased and the shape of the nuclei significantly changed for a Cu foil of lower purity (Figure 1i,j) at otherwise identical APCVD conditions. The FLG nuclei preferentially decorate Cu grain boundaries and appear aligned along the rolling striations of the foil. We find that a variation from 25 to 100 μm in foil thickness does not appear to influence the kinetics of graphene formation on that scale (Figure 1c−f), but the foil thickness does influence the Cu grain growth kinetics as discussed below.

Figure 2 shows the results of EBSD analysis marked across SEM images of Cu foil surfaces for various process stages and conditions, highlighting the effects of Cu recrystallization and grain growth. Rolling striations are a dominant feature of the as-received Cu foils, for which EBSD shows Cu grain sizes <2 μm with diverse surface orientations (Figure 2a; Table S1, Supporting Information). We find the detailed deformation texture of the used commercial cold-rolled Cu foils to vary, despite being advertised as the same product. Hence, the starting point cannot be automatically assumed as constant. It should be noted that here we do not use any additional Cu surface treatment procedure, such as electropolishing.[18] After annealing in H_2 at 1000 °C, the Cu grain sizes increase to ~50−500 μm for APCVD and ~50 μm−2 mm for LPCVD conditions (Figure 2b,c), which exceed the foil thickness. While for APCVD we still find a crystallographically diverse Cu surface (Figure 2b), the texture after LPCVD annealing becomes (111)-dominated (Figure 2c). The surface topography appears rougher and stepped for LPCVD conditions (Figure 2c inset, with individual step heights of ~10−50 nm) compared to the relatively smooth surface seen for APCVD conditions. The Cu grain size and orientation distributions are similar before and after hydrocarbon exposure (Figure 2d,e); most notably, a (111)-dominated texture for LPCVD conditions is maintained and several orientations are seen for APCVD. A polycrystalline material has no equilibrium structure, but depending on processing reaches a metastable equilibrium where the total grain boundary energy is locally minimized. At the given conditions, recrystallization followed by normal and abnormal grain growth is expected,[19] and Figure 2 is consistent with that.

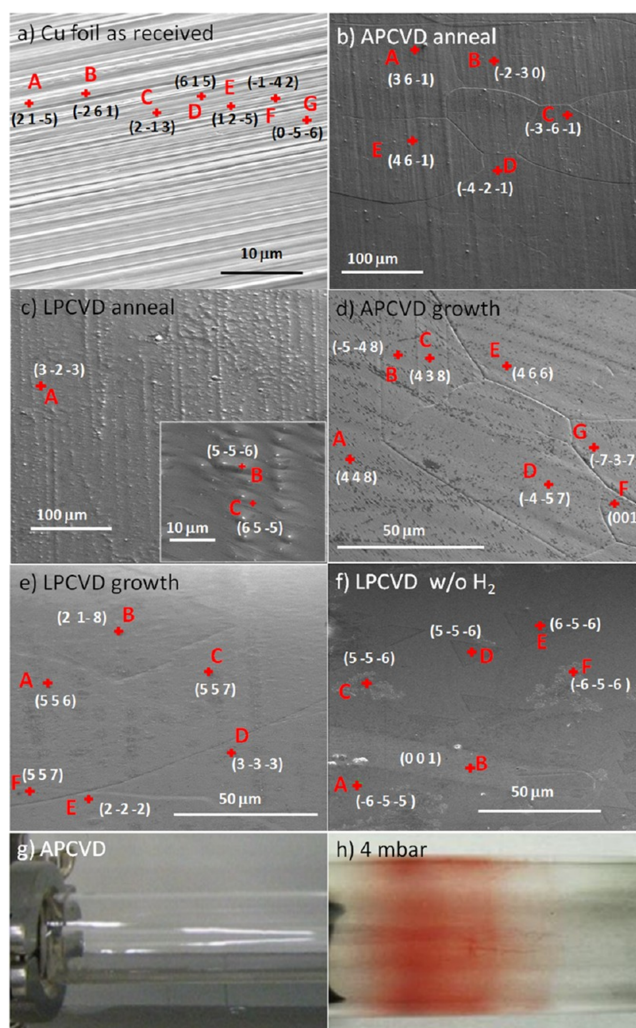

Figure 2. SEM images with EBSD in spot mode showing the evolution of the Cu catalyst for different growth conditions: (a) as received 99.999% pure 25 μm foil, (b) after APCVD annealing for 10 min at 1000 °C, (c) after LPCVD annealing for 10 min at 1000 °C min at 4 mbar, (d) after APCVD growth at 1000 °C, 1:25 CH_4/H_2 for 5 min, (e) after LPCVD growth at 1000 °C, 4 mbar, 1:5 CH_4/H_2 for 30 min, (f) after LPCVD growth at 1000 °C, 4 mbar, 1:0 CH_4/H_2 for 30 min. Optical images of the furnace tube after processing at (g) APCVD and (h) at 4 mbar and 1000 °C.

Our data emphasize that the Cu catalyst template is not static and that the involved kinetics of grain growth are highly process dependent, making this an important process step for controlled graphene CVD.

We note that most literature directed toward the optimization of uniform MLG CVD focuses on low-pressure conditions in the millibar range[9,17] during H_2 pretreatment and CH_4/H_2 exposure, similar to our LPCVD conditions of Figures 1 a,b and 2e. On the basis of their prevalence, we choose these LPCVD conditions as the standard "reference" for our further parametric study. Our discussion below will highlight why achieving continuous MLG films based on APCVD is challenging using CH_4 as the precursor. Figure 3 highlights the quality of graphene grown at our reference CH_4-based LPCVD conditions. Figure 3a shows an optical image of as-grown MLG transferred to a SiO_2 (300 nm)/Si substrate. A corresponding Raman spectrum in Figure 3b with G (≈1600 cm^{-1}, fwhm ≈ 23−25 cm^{-1}), D (≈1360 cm^{-1}), and 2D (≈2700

dx.doi.org/10.1021/jp303597m | J. Phys. Chem. C 2012, 116, 22492−22501

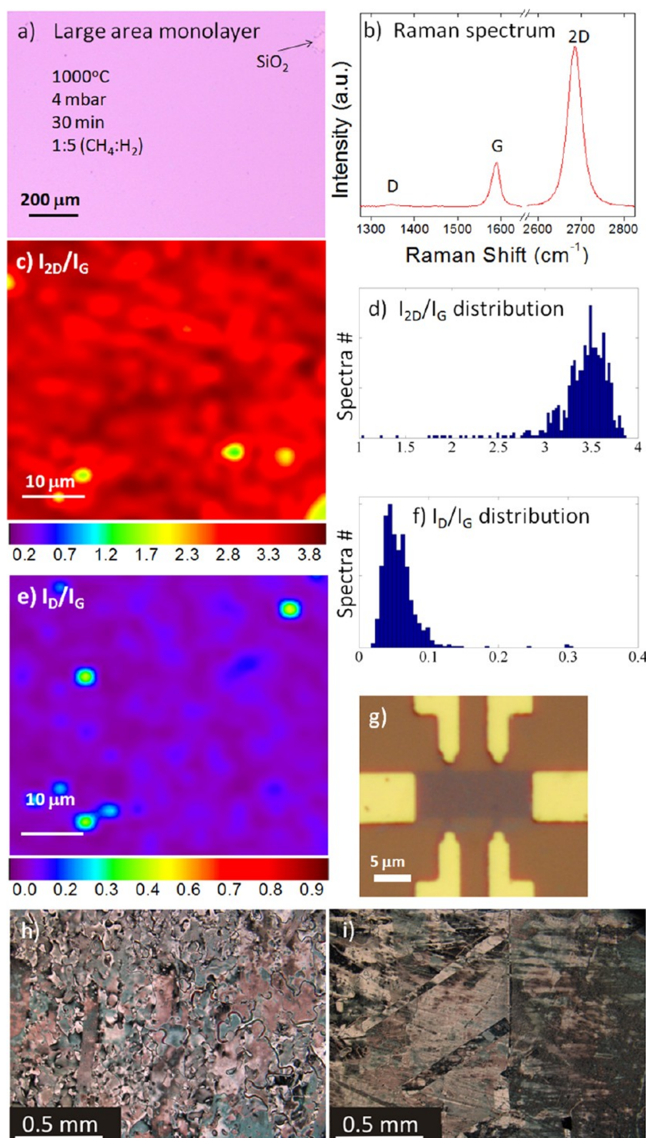

Figure 3. Characterization of a large-area MLG film grown in LPCVD, 4 mbar, 1000 °C, 1:5 CH_4/H_2 for 30 min, on 99.999% pure 25 μm foil: (a) optical image, (b) Raman spectrum confirming the presence of MLG. Raman map of large-area MLG (c) I_{2D}/I_G and (e) I_D/I_G. (d) and (f) show the corresponding distribution statistics. (g) Six contact Hall geometry devices. (h) Control POM image in a region of the sample containing no graphene. (i) POM image for a liquid crystal (LC) over graphene sample.

cm^{-1}, fwhm ≈ 35−37 cm^{-1}, which can be fitted with a single Lorentzian function) peaks as well as an I_{2D}/I_G ratio of ≈3.5 and I_D/I_G ratio of ≈0.05 demonstrate the high quality of the MLG.[3,20] Parts c and e of Figure 3 show Raman I_{2D}/I_G and I_D/I_G maps of the MLG (dimensions 50 μm × 50 μm), respectively, along with the corresponding distribution statistics (Figure 3d,f). The maps show average values of $I_{2D}/I_G \approx 3.5$ and $I_D/I_G \approx 0.05$ over a large area. Six contact Hall geometry devices (Figure 3g) give sheet resistances (on a SiO_2 support) in the range of 400−800 Ω/□ and mobilities in the 2000−3000 cm^2 V^{-1} s^{-1} range (with a p doping of a few 10^{12} cm^{-2}). To characterize sample uniformity and polycrystallinity over larger areas, we validate the potential of a liquid crystal based polarizing optical microscopy technique as recently reported by Kim et al.[15] Parts h and i of Figure 3 show polarizing optical microscopy (POM) images of an empty control and our reference MLG, respectively. The POM contrast is based on sample interactions with a 5CB nematic liquid crystal (see the Supporting Information). Across a 1 cm^2 MLG area, POM indicates feature sizes ranging from ~40 μm^2 to a few hundred square micrometers, which is consistent with the observed nucleus sizes of ~30−40 μm^2 in Figure 1 and the subsequent merging of domains with roughly similar orientations. We note that all characterization above is done after graphene transfer; i.e., it includes possible degradation incurred during transfer.

Whereas "optimized" CVD parameters can be highly system specific, we note that the variation of key parameters over a wide range offers fundamental insights into the growth process and allows the establishment of more generic growth guidelines. Figure 4 shows results of our systematic exploration of the wider CVD parameter space and focuses on the effects of total pressure, growth time, and hydrocarbon partial pressure, where for each experiment only one specified parameter was varied starting from the LPCVD benchmark recipe (see Figure 3). The results are presented in terms of optical images of as-grown graphene films transferred to SiO_2 (300 nm)/Si (Figure 4a−f) and corresponding Raman spectra (Figure 4g). For a lower total pressure of 1 mbar only MLG and no FLG is observed, but for the given exposure the film has large holes (Figure 4a). This is indicative of a lower graphene nucleation density and growth rate. We note that rather than focusing only on the carbon precursor and carbon addition, also competing etching processes, e.g., by H_2 or H_2O, have to be considered.[21,22] We clearly observe that as-grown graphene on Cu is etched while annealing in a H_2 atmosphere, which is the main reason why we do not use hydrogen during cooldown, in contrast to other studies.[23] We note that although this etching occurs in the presence of H_2 (at sufficiently high partial pressures), it may also arise from residual water or oxygen contamination.[8] A total pressure of 8 mbar on the other hand leads to a significant increase in FLG nucleation and film inhomogeneity. An analogous behavior is seen for an increase in the CH_4 partial pressure (Figures 3a and 4e,f), where 1:10 CH_4/H_2 results in incomplete MLG coverage and a 1:1 ratio shows significant multilayer coverage. In general, the lower the carbon precursor pressure, the lower the likelihood of achieving complete MLG surface coverage.

Parts c and d of Figure 4 combined with the reference sample in Figure 3a show the effect of growth time: the longer the growth time, the more complete the graphene coverage. Extended exposures, however, increase the fractional multilayer coverage. Importantly, we find that new graphene layers can nucleate after the completion of a monolayer. We refer to this as secondary nucleation, as compared to the primary nucleation discussed above. In this context, we note that in Figure 4b,d,f the nucleation pattern of multilayered graphene appears to follow the rolling striations of the Cu foil. Figure 4g shows that the interpretation of optical contrast in Figure 4a−f is in full agreement with measured Raman spectra corresponding to monolayer ($I_{2D}/I_G > 2$), and bilayer ($I_{2D}/I_G \approx 1$) and multilayer ($I_{2D}/I_G < 1$) graphene. Furthermore, the Raman measurements in Figure 4g also confirm the interpretation of SEM contrast regarding multilayer graphene primary nucleation for APCVD conditions in Figure 1e−h. The bilayer and FLG seen in areas of Figure 4d−f show Raman spectra (Figure 4g) corresponding to turbostratic graphene with 2D peaks that can be fitted with single Lorentzian peaks, whereas the APCVD conditions show a Raman signature consistent with Bernal stacking.[20]

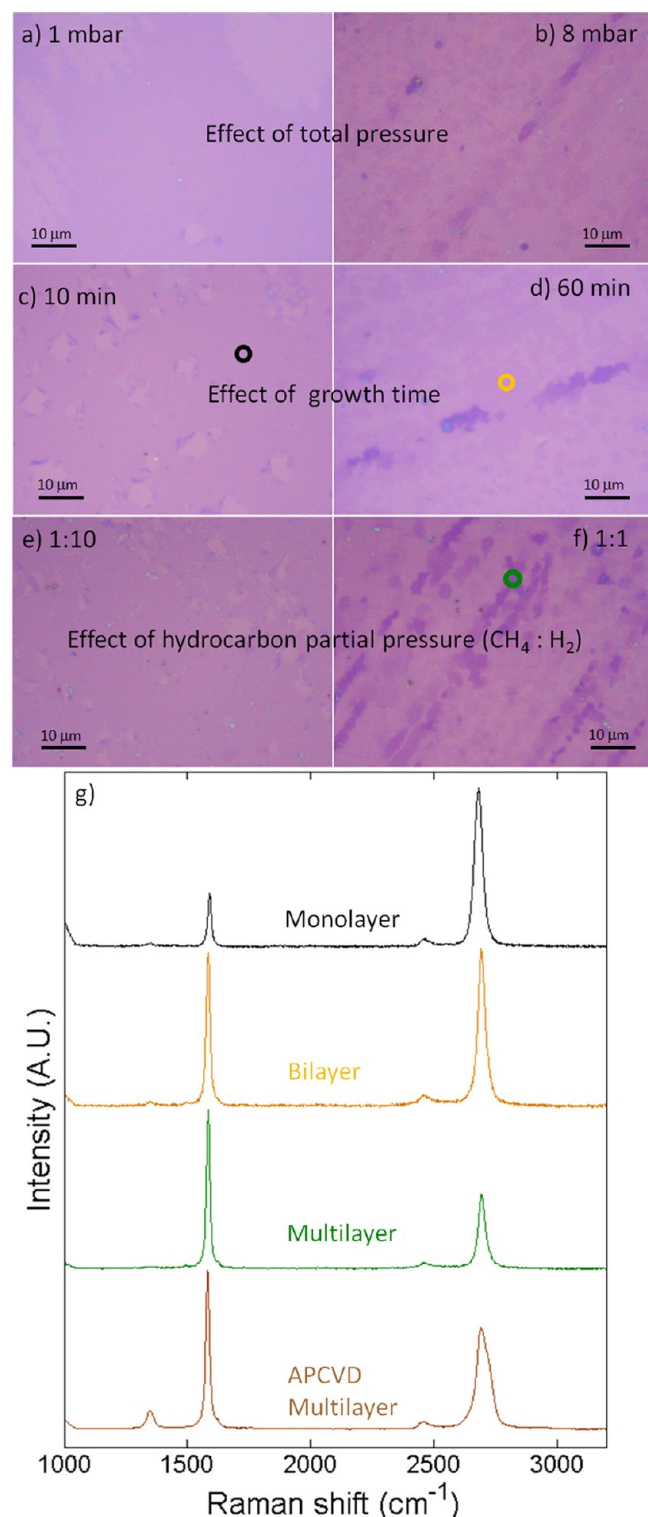

Figure 4. Optical image of a graphene film grown on 99.999% pure 25 μm foil by LPCVD and transferred to SiO_2 (300 nm)/Si at (a) 1 mbar and (b) 8 mbar at 1000 °C, 1:5 CH_4/H_2 for 30 min, for (c) 10 min and (d) 60 min at 4 mbar, 1000 °C, 1:5 CH_4/H_2, and with (e) 1:10 and (f) 1:1 CH_4/H_2, 4 mbar, 1000 °C, for 30 min. (g) Raman spectra for mono-, bi-, and multilayers seen in (a)−(f) marked with the corresponding color of the circle and APCVD FLG graphene seen in Figure 1g−j.

Figure 5 shows the results of LPCVD in undiluted CH_4 to assess the role of hydrogen dilution during growth in more detail. The postgrowth Cu surface is dominated by triangular and other three lobed structures (Figure 5a−d), partly resembling a Sierpinski triangle like fractal pattern. An EBSD analysis (Figure 2f) shows a predominant (111) texture for the processed Cu foil, whereby the triangles and lobed structures formed on Cu(111) facets and are not present on Cu(001). Attempts to transfer the structures to SiO_2/Si substrates resulted in small discontinuous patches of graphene and residual PMMA. Raman confirms the transferred patches as MLG (Figure 5f). Importantly, Raman spectra (457 nm excitation) measured directly on the processed Cu foil show peaks corresponding to CuO (300 and 652 cm^{-1})[24,25]and CuO_2 (217, 415, 504, and 808 cm^{-1})[24,25] for the triangular areas. The mechanisms of this self-organization are unclear, but we suggest it arises on the basis of the balance of three competing processes, namely, graphene formation, its etching by residual oxygen, and the formation of copper oxide from this residual oxygen. The parallel processes of reduction and oxidation could make the copper oxide species extremely mobile, causing them to self-align in a triangular fashion due to the 3-fold symmetry of Cu(111).[26,27] Hence, our data show that the presence of a hydrogen atmosphere suppresses the formation of copper oxide from trace oxygen contamination during CVD. We note that the observation of triangular graphene on Cu(111) has been reported in recent literature,[26] without however considering the role of oxygen. This highlights why CH_4 as precursor requires H_2 dilution, and our data above emphasize the delicate effects of the CH_4/H_2 balance.

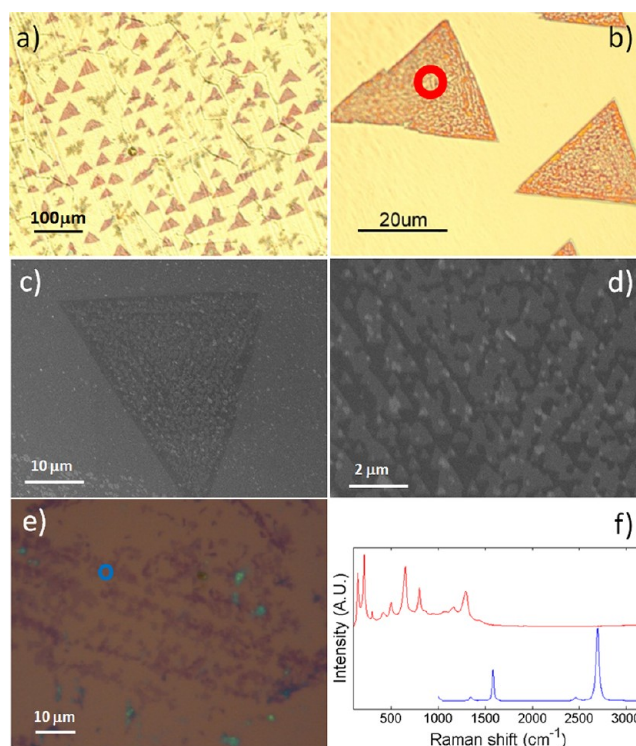

Figure 5. LPCVD growth in the absence of H_2 at 4 mbar, CH_4/H_2 (1:0), 1000 °C, for 30 min: (a, b) optical images of Cu foil postgrowth; (c, d) SEM images of Cu foil postgrowth; (e) optical images post-transfer to SiO_2 (300 nm)/Si wafer; (f) Raman spectra measured on the triangular structure on the Cu foil (red, 457 nm laser) and post-transfer to SiO_2 (300 nm)/Si wafer (blue).

Figure 2h shows that for LPCVD conditions at 1000 °C the rate of Cu sublimation is significant and deleterious. Increasing

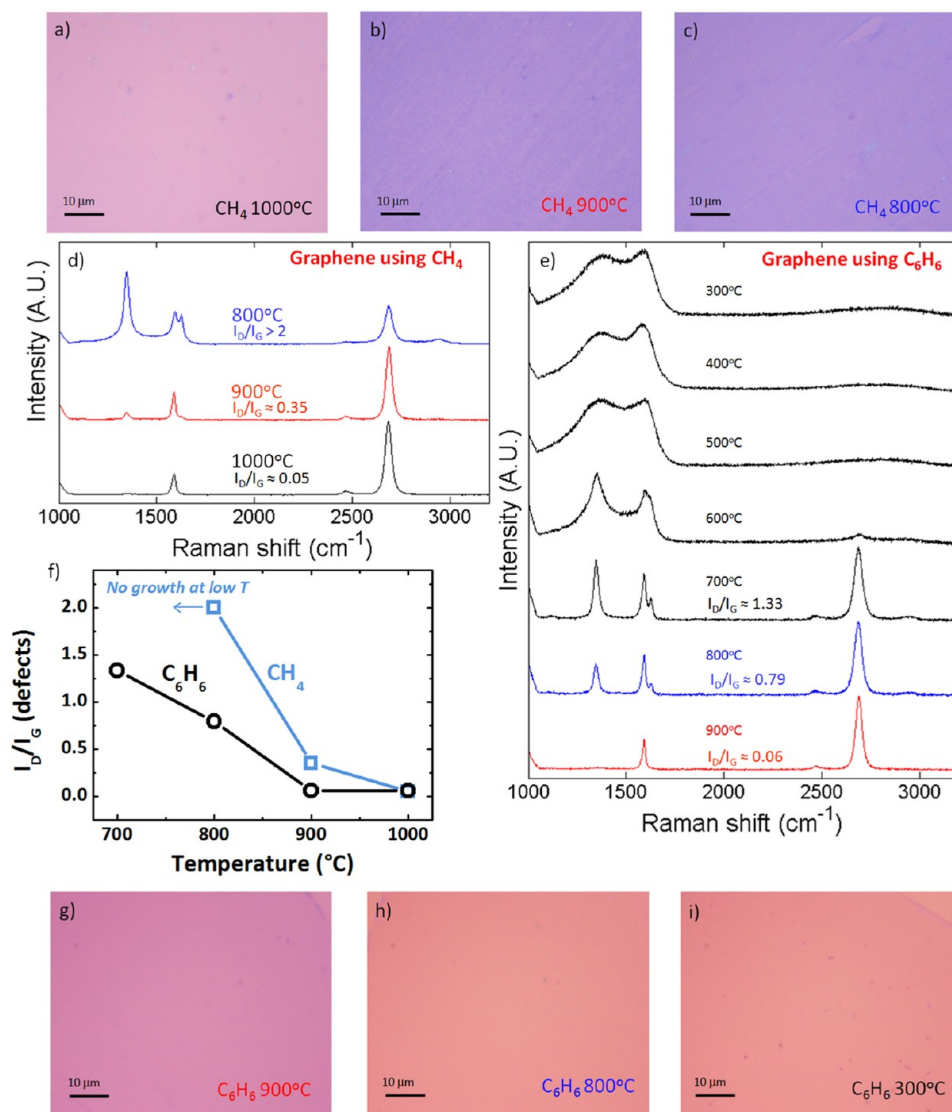

Figure 6. Optical images of a graphitic film grown on Cu at 4 mbar, 1:5 CH_4/H_2, 30 min, at (a) 1000, (b) 900, and (c) 800 °C. (d) shows the corresponding Raman spectra marked with the respective color. (e) shows Raman spectra measured on graphitic films grown with C_6H_6 at different temperatures post-transfer to a SiO_2 (300 nm)/Si wafer. (f) I_D/I_G ratios for graphitic films grown from CH_4 (squares) and C_6H_6 (circles). Optical images of a graphitic film grown on Cu with C_6H_6 at (g) 900, (h) 800, and (i) 300 °C post-transfer to a SiO_2 (300 nm)/Si wafer.

the total pressure with an inert diluent can suppress the Cu sublimation, but as discussed below, maintaining the CH_4/H_2 balance and achieving complete MLG coverage then becomes increasingly challenging.[28] The exponential variation of vapor pressure with temperature strongly motivates a temperature reduction to mitigate the Cu sublimation. Parts a−d of Figure 6 show the effect of lowering the process temperature for CH_4-based graphene CVD on Cu. Comparing graphitic films grown at 1000, 900, and 800 °C, the optical images of the transferred films all appear homogeneous (Figure 6a−c). The corresponding Raman spectra, however, show a significant deterioration in graphene quality, as highlighted by the significantly increased D peak intensity. The spectrum for 900 °C shows an I_{2D}/I_G ratio of ∼2.5 and I_D/I_G ratio of ∼0.35. Also observed is the emergence of an additional defect peak, referred to as the D′ peak,[29] near the G peak at higher wavenumbers. A further reduction in temperature to 800 °C leads to $I_{2D}/I_G \approx 1.2$ and $I_D/I_G > 2$ and a D′ peak intensity increased to the level of I_G. We also note that all these films are continuous, in contrast to recent literature that claims that no continuous films can be obtained below 1000 °C at comparable experimental conditions.[23] Whereas the parameters discussed in Figure 4 mainly influence the M/FLG ratio and coverage, the growth temperature is clearly the most significant parameter influencing the crystalline quality of the as-grown material. Our data show that with CH_4 as precursor the growth temperature cannot be lowered sufficiently to mitigate Cu sublimation and at the same time maintain a high graphene quality.

This raises the question of what fundamentally determines at how low a temperature high-quality graphene CVD can be grown. We approach this question here by using benzene (C_6H_6) as an alternative carbon precursor. Figure 6e shows the results of LPCVD, for which a simple exposure to undiluted C_6H_6 was adopted. At 900 °C, highly uniform MLG films of high quality ($I_D/I_G \approx 0.06$, Figure 6e) are achieved with greatly reduced Cu sublimation compared to 1000 °C. As in Figure 6d, the graphene quality decreases with decreasing growth temperature (Figure 6 e). However, the MLG quality for

dx.doi.org/10.1021/jp303597m | J. Phys. Chem. C 2012, 116, 22492−22501

C_6H_6-based CVD is better at any given temperature (compare parts d and e of Figure 6), and unlike for CH_4, graphitic material (albeit highly defective) nucleates at temperatures as low as 600 °C for C_6H_6. Figure 6f directly compares the measured I_D/I_G ratios for the two different carbon precursors. Raman maps for the C_6H_6-derived MLG at 900 °C show a uniform $I_D/I_G \approx 0.06$ and $I_{2D}/I_G \approx 2.5$ distribution over a large area (dimensions 50 μm × 50 μm) as seen in Figure 7a–d. POM indicates a similar grain size distribution and polycrystallinity for the C_6H_6-derived MLG films (Figure 7i,j) as compared to the reference samples for CH_4/H_2-based CVD (Figure 3h,i). Furthermore, six contact Hall geometry devices based on graphene grown from C_6H_6 at 900 °C give sheet resistances (on a SiO_2 support) in the range of 400–800 Ω/□ and mobilities in the 2000–3000 $cm^2\ V^{-1}\ s^{-1}$ range (with a p doping of a few $10^{12}\ cm^{-2}$). These results highlight that C_6H_6 enables similar graphene quality at 100–150 °C lower temperatures, i.e., that the apparent low-temperature limit is precursor dependent.

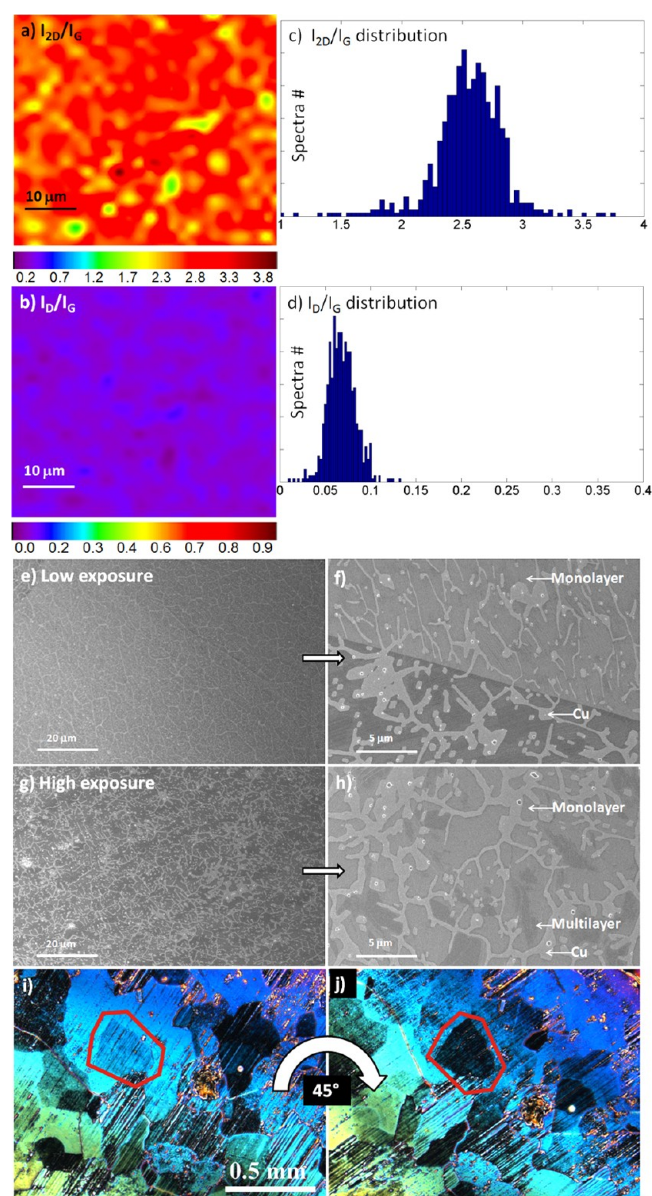

Figure 7. Raman map of large-area MLG films grown from C_6H_6 at LPCVD conditions at 900 °C on 99.999% pure 25 μm foil: (a) I_{2D}/I_G maps; (b) I_D/I_G maps. (c) and (d) show the corresponding distribution statistics. SEM images at different magnifications showing graphene nuclei on Cu from C_6H_6 at LPCVD conditions at 900 °C on 99.999% pure 25 μm foil (e, f) at low-exposure conditions with a C_6H_6 partial pressure of $\sim 10^{-4}$ mbar for 5 min and (g, h) at high-exposure conditions with a C_6H_6 partial pressure of $\sim 10^{-2}$ mbar for 5 min. (i–j) POM images for a liquid crystal (LC) over C_6H_6-derived graphene sample at different rotations highlighting the polycrystallinity of the MLG.

The variation of CVD parameters over a wider parameter space for the benzene-based process shows a similar general behavior compared to that with CH_4 as precursor (Figure 7e–h). In particular, the lower the carbon precursor partial pressure, the lower the likelihood of achieving complete MLG surface coverage, and the higher the exposure pressure, the higher the likelihood of multilayer nucleation and film inhomogeneity. Again, the growth rate depends on the specific Cu surface. However, considering that between parts e and f and parts g and h of Figure 7 the C_6H_6 partial pressure increase was ~100-fold, the increase in fractional FLG coverage and inhomogeneity is surprisingly little. Significantly, we note that the partial pressure range in which C_6H_6 yields MLG ($\sim 10^{-4}$–10^{-2} mbar) is much wider (relative to the partial pressure used) than for the CH_4 process (~0.2–1.5 mbar). Hence, for the conditions used, C_6H_6 as precursor does not require H_2 dilution and enables growth at lower temperatures with more robust processing conditions.

■ DISCUSSION

The overall CVD process for graphene growth can be discussed in the context of basic heterogeneous catalysis and 2D crystal growth kinetics as a multistep reaction comprising (1) gaseous precursor transport to and dissociation on the catalyst surface, (2) transport of carbon (species) on the surface and into/out of the bulk of the catalyst, (3) graphene nucleation and carbon incorporation into the growing graphene layer, and (4) etching of the as-formed graphene. Step 1 thereby comprises transport of gas reactants through the boundary layer above the catalyst surface and the adsorption/desorption kinetics of the catalytic reaction. Simultaneous to its formation, graphene etching can occur (step 4), depending on the composition of the gas atmosphere and the presence of contaminants in the CVD setup/process. The thermodynamic driving force for growth, i.e., step 3, is a carbon supersaturation at the catalyst surface.[16] In CVD this supersaturation is created via step 1, whereby the different CVD conditions can be expressed as different carbon chemical potentials. The chemical potential depends on the temperature and partial pressures, which in turn depend on the choice of precursor and the reaction considered. A more reactive carbon source corresponds to carbon supplied at a higher chemical potential. We adopt this general framework here to qualitatively rationalize our findings, even though the experimental conditions might not be close to equilibrium; i.e., the carbon chemical potential is difficult to quantify.[30]

For carbon supplied at a very high chemical potential, graphene growth is very favorable and can become nonspecific to details of the catalyst surface. Our data here (Figures 1, 4, and 7) are consistent with such a generic behavior insofar that the higher the supplied carbon chemical potential, the higher the likelihood of film inhomogeneity and primary and secondary multilayer nucleation. Assuming growth occurs isothermally during CVD exposure and not during cooldown and that additional layers grow in contact with the catalyst, i.e.,

underneath the existing graphene,[31,32] secondary nucleation indicates that carbon reaches the Cu surface even after complete MLG coverage. Isolated graphene flakes have been shown to be impermeable to gases;[33] hence, we suggest that the observed carbon leakage is due to the inherent polycrystallinity of as-grown MLG whereby the domain boundaries and other defects offer pathways for the precursor to reach the catalyst. Hence, clearly graphene CVD on Cu cannot be expected to inherently (independent of the conditions applied) give a self-limiting homogeneous monolayer coverage. We emphasize that this has important ramifications for FLG CVD. Primary nucleation will not give a homogeneous FLG coverage due to the different growth rates of the layers. Secondary nucleation will require leakage through the covering layer(s), and the challenge is thereby to feed homogeneous growth through inhomogeneous leakage. Furthermore, we expect the leakage to significantly decrease with the number of layers, so the number of layers possible is clearly limited by this method.

The more the supplied carbon chemical potential is lowered, the more specific the graphene formation becomes to details of the catalyst surface, nature of nucleation sites, energy costs associated with graphene edges, and, for instance, additional strain energies depending on the lattice mismatch.[30] Figures 1 and 7 highlight that graphene formation is indeed dependent on the catalyst surface orientation and impurity levels. Improved growth on Cu(111) has been previously attributed to improved precursor adsorption and high diffusion of carbon species.[34] Compared to, for instance, Ni, Cu in its given metallic state is a less active catalyst for step 1; hence, higher temperatures are required to supply carbon at a given rate. Compared to CH_4, C_6H_6 represents a more reactive carbon source, which is captured in the temperature dependence of Figure 6. Hence, it is not surprising that we do not see any graphitic deposits at temperatures below 700 °C for CH_4, whereas for C_6H_6 we observe carbon film deposition at temperatures as low as 300 °C (see Figure 6e) on Cu for the given conditions. Below 600 °C, the crystallinity of the as-grown carbon is poor, and although the defect density will again depend on the detailed growth kinetics (e.g., carbon arrival rate vs incorporation rate), we cannot reproduce the Cu-catalyzed growth of graphene at a temperature of 600 °C or below, as recently reported for toluene[18] (~600 °C, $I_D/I_G \approx 0.35$) and ill-defined C_6H_6 exposures in hot-wall furnaces.[35] We note in this context that these previous efforts have focused on lowering the temperature, but clearly compromised on graphene quality.[18,35] Bearing in mind that graphene has to be transferred off the catalyst metal for most applications,[36] our motivation here is a temperature reduction while maintaining the quality.

Our data indicate that C_6H_6 as precursor enables not only growth at lower temperatures but also more robust processing conditions. Some previous literature suggests that the six-membered ring configuration of benzene would provide an inherent advantage that could help to explain our findings.[35] However, even though the detailed nature of carbon species in steps 2 and 3 remains unknown, we see no evidence that the six-membered ring configuration of C_6H_6 will be preserved at step 1 for the given conditions, as sometimes suggested in the literature.[35,37] Rather, we suggest that the advantage of C_6H_6 lies in the rate balance that it allows during CVD. CH_4 requires H_2 dilution to reduce the Cu surface (Figure 5), and the required CH_4/H_2 balance is critical (Figure 4). We show that a lower CH_4/H_2 ratio leads to etching; hence, the CH_4/H_2 balance reflects a balance between carbon deposition and etching, i.e., between steps 3 and 4. We emphasize that this balance is highly process parameter dependent, which is why CH_4-based CVD is more delicate to control. At APCVD conditions, for instance, well-known CVD kinetic models predict a mass transfer limited regime, whereby the boundary layer in step 1 is rate limiting. This has also been discussed in the context of graphene APCVD.[28] On the basis of our data, we suggest here that the delicate CH_4/H_2 balance shifts for pressure-induced changes of the boundary layer, and this is why achieving continuous MLG films based on APCVD is very challenging using CH_4 as precursor. C_6H_6 as precursor on the other hand is more reactive and requires no reactive diluent and related delicate balancing. We also suggest that diluting C_6H_6 with a neutral gas such as Ar should be much more straightforward than for CH_4 in terms of maintaining high-quality graphene growth.

The above argumentation assumes that the observed graphene formation on Cu occurs predominantly during the precursor exposure at isothermal conditions, rather than due to precipitation upon cooling.[7,8] This assumption is supported by in situ observations of isothermal graphene growth on Cu during elemental carbon deposition;[38] however, the importance of the contribution of carbon precipitation on cooling should also be considered. On the basis of a simplistic consideration of carbon solubility in Cu at 1000 °C of between 0.00070 atom %[39] and 0.028 atom %,[40] the amount of carbon dissolved in the 25 μm foil corresponds to between 0.4 and 15.5 layers of graphene with an atomic density of 3.8×10^{19} carbon atoms m^{-2}. It should be noted that the large uncertainties here reflect the significant disparities between the solubility values reported in the literature.[39,40] Realistically, the diffusion lengths of carbon dissolution and precipitation may limit the active volume to some fraction of the foil thickness and should be considered when estimating whether the quantity of carbon that precipitates as graphene upon cooling is significant.[8] For such a calculation to be informative, a validation of the solubility and diffusivity of carbon in Cu is required, which lies beyond the scope of the present work. We note that further in situ experiments are needed to fully clarify the relative importance of growth by precipitation upon cooling.

■ CONCLUSIONS

We systematically explored the parameter space of graphene CVD on polycrystalline Cu foils in particular regarding the choice of carbon precursor and mitigation of Cu sublimation as required for industrial manufacture. CH_4, the currently most widely used carbon precursor, requires H_2 dilution and high temperatures (1000 °C) to keep the Cu surface reduced and yield high-quality graphene. The H_2 atmosphere etches as-grown graphene; hence, maintaining a balanced CH_4/H_2 ratio is critical. Such balance is more easily achieved at low-pressure conditions, at which however Cu sublimation is at deleterious levels. In contrast, C_6H_6 as precursor requires no reactive dilution, i.e., no delicate balance to be maintained, and consistently gives similar graphene quality at 100−150 °C lower temperatures compared to CH_4-based CVD. The lower process temperature and more robust processing conditions allow the problem of Cu sublimation to be effectively addressed. Our growth study shows that Cu is not inherently limiting graphene formation to a monolayer. Rather, the higher the supplied carbon chemical potential, the higher the likelihood of film inhomogeneity and primary and secondary

multilayer nucleation. Secondary nucleation indicates that carbon reaches the Cu surface even after complete MLG coverage, whereby we suggest that the domain boundaries of the inherently polycrystalline layers offer pathways for the precursor to reach the catalyst. Our data further emphasize that the Cu catalyst template is not static and that the involved kinetics of grain growth are highly process dependent, making this an important process step for controlled graphene CVD.

Although the data presented concern only two carbon precursors, we expect the insights achieved to be of general relevance for the optimization of graphene CVD and more rational process design. While C_6H_6 may not be the precursor of choice for industrial upscaling due to its harmful effects on health, we think that it serves as a good model precursor system to effectively study the effect of precursor reactivity for graphene CVD. We have preliminary data for xylene as the carbon precursor, which is an example of a cheap and safe precursor that shows advantages similar to those highlighted here for benzene, in particular giving MLG at 900 °C when diluted in Ar at APCVD conditions without Cu sublimation.

■ ASSOCIATED CONTENT

Supporting Information

More experimental details on the EBSD analysis and on the liquid crystal based POM technique. This material is available free of charge via the Internet at http://pubs.acs.org.

■ AUTHOR INFORMATION

Corresponding Author

*E-mail: sh315@cam.ac.uk.

Notes

The authors declare no competing financial interest.

■ ACKNOWLEDGMENTS

S.H. acknowledges funding from ERC Grant InsituNANO (279342) and from EPSRC (Grant EP/H047565/1). This research was partially supported by the EU FP7 under GRAFOL(285275). P.R.K. acknowledges funding from the Cambridge Commonwealth Trust, and C.D. acknowledges funding from the Royal Society. We acknowledge Dr. Matt Cole for help with equipment modification, Amalya Kostanyan for help with the POM characterization, and Dr. Bernhard C. Bayer for discussions.

■ REFERENCES

(1) Dresselhaus, M. S.; Dresselhaus, G.; Avouris, P. *Carbon Nanotubes: Synthesis, Structure, Properties, and Applications*; Springer: Berlin, 2001.

(2) Hiruma, K.; Yazawa, M.; Katsuyama, T.; Ogawa, K.; Haraguchi, K.; Koguchi, M.; Kakibayashi, H. *J. Appl. Phys.* **1995**, *77*, 447−62.

(3) Hofmann, S.; Sharma, R.; Ducati, C.; Du, G.; Mattevi, C.; Cepek, C.; Cantoro, M.; Pisana, S.; Parvez, A.; Cervantes-Sodi, F.; et al. *Nano Lett.* **2007**, *7*, 602−8.

(4) Li, X.; Cai, W.; An, J.; Kim, S.; Nah, J.; Yang, D.; Piner, R.; Velamakanni, A.; Jung, I.; Tutuc, E.; et al. *Science* **2009**, *324*, 1312−4.

(5) Bae, S.; Kim, H.; Lee, Y.; Xu, X.; Park, J. S.; Zheng, Y.; Balakrishnan, J.; Lei, T.; Kim, H. R.; Song, Y. I.; et al. *Nat. Nanotechnol.* **2010**, *5*, 574−8.

(6) Li, X.; Cai, W.; Colombo, L.; Ruoff, R. S. *Nano Lett.* **2009**, *9*, 4268−72.

(7) Weatherup, R. S.; Bayer, B. C.; Blume, R.; Ducati, C.; Baehtz, C.; Schlögl, R.; Hofmann, S. *Nano Lett.* **2011**, *11*, 4154−60.

(8) Weatherup, R. S.; Bayer, B. C.; Blume, R.; Baehtz, C.; Kidambi, P. R.; Fouquet, M.; Wirth, C. T.; Schlögl, R.; Hofmann, S. *ChemPhysChem* **2012**, *10*, 2544−49.

(9) Regmi, M.; Chisholm, M. F.; Eres, G. *Carbon* **2012**, *50*, 134−141.

(10) Huang, P. Y.; Ruiz-Vargas, C. S.; Zande, A. M.; van der; Whitney, W. S.; Levendorf, M. P.; Kevek, J. W.; Garg, S.; Alden, J. S.; Hustedt, C. J.; Zhu, Y.; et al. *Nature* **2011**, *469*, 389−92.

(11) Kim, K.; Lee, Z.; Regan, W.; Kisielowski, C.; Crommie, M. F.; Zettl, A. *ACS Nano* **2011**, *5*, 2142−6.

(12) Petrone, N.; Dean, C. R.; Meric, I.; Zande, A. M.; van der; Huang, P. Y.; Wang, L.; Muller, D.; Shepard, K. L.; Hone, J. *Nano Lett.* **2012**, *12*, 2751−6.

(13) Li, X.; Magnuson, C. W.; Venugopal, A.; Tromp, R. M.; Hannon, J. B.; Vogel, E. M.; Colombo, L.; Ruoff, R. S. *J. Am. Chem. Soc.* **2011**, *133*, 2816−9.

(14) Ismach, A.; Druzgalski, C.; Penwell, S.; Schwartzberg, A.; Zheng, M.; Javey, A.; Bokor, J.; Zhang, Y. *Nano Lett.* **2010**, *10*, 1542−8.

(15) Kim, D. W.; Kim, Y. H.; Jeong, H. S.; Jung, H.-T. *Nat. Nanotechnol.* **2012**, *7*, 29−34.

(16) Batzill, M. *Surf. Sci. Rep.* **2012**, *67*, 83−115.

(17) Li, X.; Magnuson, C. W.; Venugopal, A.; An, J.; Suk, J. W.; Han, B.; Borysiak, M.; Cai, W.; Velamakanni, A.; Zhu, Y.; et al. *Nano Lett.* **2010**, *10*, 4328−34.

(18) Zhang, B.; Lee, W. H.; Piner, R.; Kholmanov, I.; Wu, Y.; Li, H.; Ji, H.; Ruoff, R. S. *ACS Nano* **2012**, *6*, 2471−76.

(19) Humphreys, F. J.; Hatherly, M. *Recrystallization and Related Annealing Phenomena*; Elsevier: Amsterdam, 2004.

(20) Ferrari, A. C.; Meyer, J. C.; Scardaci, V.; Casiraghi, C.; Lazzeri, M.; Mauri, F.; Piscanec, S.; Jiang, D.; Novoselov, K. S.; Roth, S. *Phys. Rev. Lett.* **2006**, *97*, 187401.

(21) Zhang, Y.; Li, Z.; Kim, P.; Zhang, L.; Zhou, C. *ACS Nano* **2012**, *6*, 126−32.

(22) Vlassiouk, I.; Regmi, M.; Fulvio, P.; Dai, S.; Datskos, P.; Eres, G.; Smirnov, S. *ACS Nano* **2011**, *5*, 6069−76.

(23) Kim, H.; Mattevi, C.; Calvo, M. R.; Oberg, J. C.; Artiglia, L.; Agnoli, S.; Hirjibehedin, C. F.; Chhowalla, M.; Saiz, E. *ACS Nano* **2012**, *6*, 3614−23.

(24) Rackauskas, S.; Nasibulin, A. G.; Jiang, H.; Tian, Y.; Kleshch, V. I.; Sainio, J.; Obraztsova, E. D.; Bokova, S. N.; Obraztsov, A. N.; Kauppinen, E. I. *Nanotechnology* **2009**, *20*, 165603.

(25) Hamilton, J. C. *J. Electrochem. Soc.* **1986**, *133*, 739.

(26) Liu, J.; Wu, J.; Edwards, C. M.; Berrie, C. L.; Moore, D.; Chen, Z.; Maroni, V. A.; Paranthaman, M. P.; Goyal, A. *Adv. Funct. Mater.* **2011**, *21*, 3868−3874.

(27) Wiame, F.; Maurice, V.; Marcus, P. *Surf. Sci.* **2007**, *601*, 1193−1204.

(28) Bhaviripudi, S.; Jia, X.; Dresselhaus, M. S.; Kong, J. *Nano Lett.* **2010**, *10*, 4128−4133.

(29) Cançado, L. G.; Jorio, A; Ferreira, E. H. M.; Stavale, F.; Achete, C. A; Capaz, R. B.; Moutinho, M. V. O.; Lombardo, A; Kulmala, T. S.; Ferrari, A. C. *Nano Lett.* **2011**, *11*, 3190−6.

(30) Saadi, S.; Abild-Pedersen, F.; Helveg, S.; Sehested, J.; Hinnemann, B.; Appel, C. C.; Nørskov, J. K. *J. Phys. Chem. C* **2010**, *114*, 11221−27.

(31) Nie, S.; Wu, W.; Xing, S.; Yu, Q.; Mccarty, K. F. Growth from below: bilayer graphene on copper by chemical vapor deposition. 2012, arXiv:1202.1031v2. arXiv.org e-Print archive. http://arxiv.org/abs/1202.1031v2.

(32) Nie, S.; Walter, A. L.; Bartelt, N. C.; Starodub, E.; Bostwick, A.; Rotenberg, E.; McCarty, K. F. *ACS Nano* **2011**, *5*, 2298−306.

(33) Bunch, J. S.; Verbridge, S. S.; Alden, J. S.; Zande, A. M.; van der; Parpia, J. M.; Craighead, H. G.; McEuen, P. L. *Nano Lett.* **2008**, *8*, 2458−62.

(34) Wood, J. D.; Schmucker, S. W.; Lyons, A. S.; Pop, E.; Lyding, J. W. *Nano Lett.* **2011**, *11*, 4547−54.

(35) Li, Z.; Wu, P.; Wang, C.; Fan, X.; Zhang, W.; Zhai, X.; Zeng, C.; Li, Z.; Yang, J.; Hou, J. *ACS Nano* **2011**, *5*, 3385−90.

(36) Kidambi, P. R.; Bayer, B. C.; Weatherup, R. S.; Ochs, R.; Ducati, C.; Szabó, D. V.; Hofmann, S. *Phys. Status Solidi RRL* **2011**, *9*, 341−343.
(37) Yang, Y.; Hu, Z.; Tian, Y. J.; L, Y. N.; Wang, X. Z.; Chen, Y. *Nanotechnology* **2003**, *14*, 733−737.
(38) Wofford, J. M.; Nie, S.; McCarty, K. F.; Bartelt, N. C.; Dubon, O. D. *Nano Lett.* **2010**, *10*, 4890−96.
(39) López, G. A.; Mittemeijer, E. J. *Scr. Mater.* **2004**, *51*, 1−5.
(40) McLellan, R. B. *Scr. Metall.* **1969**, *3*, 389−391.